Journal of Computational Physics 228 (2009) 2225–2238

Contents lists available at ScienceDirect

Journal of Computational Physics

journal homepage: www.elsevier.com/locate/jcp

Parallelized Characteristic Basis Finite Element Method (CBFEM-MPI)—A non-iterative domain decomposition algorithm for electromagnetic scattering problems

Ozlem Ozgun [a,b,*,1], Raj Mittra [b], Mustafa Kuzuoglu [c]

[a] *Department of Electrical Engineering, Middle East Technical University, Northern Cyprus Campus, Kalkanli, Guzelyurt, North Cyprus, via Mersin 10, Turkey*
[b] *Electromagnetic Communication Laboratory, Pennsylvania State University, University Park, PA 16802, United States*
[c] *Department of Electrical Engineering, Middle East Technical University, 06531 Ankara, Turkey*

ARTICLE INFO

Article history:
Received 23 April 2008
Received in revised form 29 November 2008
Accepted 1 December 2008
Available online 16 December 2008

Keywords:
Characteristic basis functions
Domain decomposition (DD)
Electromagnetic scattering
Finite Element Method (FEM)
MPI library

ABSTRACT

In this paper, we introduce a parallelized version of a novel, non-iterative domain decomposition algorithm, called Characteristic Basis Finite Element Method (CBFEM-MPI), for efficient solution of large-scale electromagnetic scattering problems, by utilizing a set of *specially defined* characteristic basis functions (CBFs). This approach is based on the decomposition of the computational domain into a number of non-overlapping subdomains wherein the CBFs are generated by employing a novel procedure, which differs from all those that have been used in the past. Clearly, the CBFs are obtained by calculating the fields radiated by a finite number of dipole-type sources, which are placed hypothetically along the boundary of the conducting object. The major advantages of the proposed technique are twofold: (i) it provides a substantial reduction in the matrix size, and thus, makes use of direct solvers efficiently and (ii) it enables the utilization of parallel processing techniques that considerably decrease the overall computation time. We illustrate the application of the proposed approach via several 3D electromagnetic scattering problems.

1. Introduction

The Finite Element Method (FEM) has been widely used in the electromagnetic modeling and simulation of electromagnetic boundary value problems for several decades due to its adaptability to arbitrary geometries and material inhomogeneities. However, in applications involving electrically large objects, the FEM—together with other finite methods—yields 'large' matrices whose solution may not be feasible even on state-of-the-art computers. Although the resultant matrix is sparse and can be stored by using a compressed storage scheme, the use of iterative solvers for these matrices usually creates a heavy burden on CPU memory and time due to the slow and unstable behavior of the convergence, even when accelerated by means of preconditioners. Hence, alternative techniques, such as the domain decomposition (DD) methods, have been employed to alleviate this difficulty. A general DD approach, which is based on the divide-and-conquer philosophy, breaks down a large-scale problem into a number of small sub-problems whose solution is manageable. There are several DD strategies devised for problems governed by partial differential equations. The oldest class of the DD methods is known as Schwarz Methods [1]. The perspective of the DD method itself is very broad as a research subject, and thus, only a number of DD approaches that have been utilized in electromagnetic boundary value problems are listed in [2–10].

[*] Corresponding author. Address: Department of Electrical Engineering, Middle East Technical University, Northern Cyprus Campus, Kalkanli, Guzelyurt, North Cyprus, via Mersin 10, Turkey. Tel.: +90 392 661 2972.
E-mail addresses: ozgunozlem@gmail.com, ozozgun@metu.edu.tr (O. Ozgun).

[1] She was a Visiting Scholar with the Electromagnetic Communication Laboratory of the Pennsylvania State University, while this research was conducted.

0021-9991/$ - see front matter © 2008 Elsevier Inc. All rights reserved.
doi:10.1016/j.jcp.2008.12.002

In this paper, we present the parallelized "Characteristic Basis Finite Element Method (CBFEM-MPI)," which is a novel domain decomposition finite element algorithm for the solution of a wide class of electromagnetic boundary problems. The proposed technique is non-iterative and is well-suited to the implementation of parallel processing techniques using such as the Message Passing Interface (MPI) library [11]. Basically, this method utilizes a set of *specially defined* characteristic basis functions (CBFs) in conjunction with a domain decomposition scheme that partitions the computational domain into a number of *non-overlapping* subdomains. The CBFs—macro-domain basis functions that are constructed in each subdomain by considering the physics of the problem—have been originally proposed to solve time-harmonic electromagnetic problems in the context of the Method of Moments (MoM), by using the CBMoM (Characteristic Basis/Method of Moments) approach that have employed *overlapping* subdomains [12–14]. The CBFs have also been employed in both the FEM [15] and the Finite Difference Time Domain (FDTD) method [16], wherein the original domain has been divided into *overlapping* subdomains. However, the CBFEM-MPI is distinguished from all previous approaches because of three main reasons: (i) first, its implementation procedure is based on *non-overlapping* subdomains; (ii) second, the CBFs are generated in each subdomain by using a novel approach in which the CBFs are determined by radiating a finite number of fictitious *current-elements* (viz., *dipoles* in 3D time-harmonic case) located along the boundary of the conducting object; and finally, (iii) the CBFEM-MPI can be applied to both quasi-static and time-harmonic cases in a straightforward manner. (The quasi-static case is beyond the scope of this paper, and will be discussed elsewhere.) In this paper, we deal with the problem of electromagnetic scattering from an arbitrarily shaped conducting object. Two desirable attributes of CBFEM-MPI are: (i) it realizes a significant reduction in the matrix size in such a way that the resulting matrices can easily be handled by direct—as opposed to iterative—solvers; and, (ii) it realizes a substantial decrease in the overall computation time due to its parallelizable nature. Hence, it can handle large-scale problems in a time-efficient manner when run on multiple processors.

This paper is structured as follows: In Section 2, we present the theoretical formulation of the CBFEM-MPI approach in detail, along with its basic principles of implementation and its parallelized architecture. In Section 3, we present several numerical applications that demonstrate the performance of the method in the context of the 3D electromagnetic scattering problems involving a variety of arbitrarily shaped objects. Finally, we draw some conclusions in Section 4 with regard to the salutary features of the technique proposed in this paper.

2. CBFEM-MPI algorithm

We illustrate the original scattering problem as shown in Fig. 1(a). The open-region geometry of the problem is simulated by terminating the computational domain with a perfectly matched layer (PML), which is implemented by the locally conformal PML approach [17,18]. The electromagnetic scattering problem involving a perfectly conducting object (or scatterer) can be expressed as a boundary value problem governed by the vector wave equation with given boundary condition (BC) as follows

$$\nabla \times \nabla \times \vec{E}^s - k^2 \vec{E}^s = 0 \quad \text{in } \Omega_{\mathrm{FS}} \tag{1.a}$$

$$\text{with BC} : \hat{n} \times \vec{E}^s = -\hat{n} \times \vec{E}^{inc} \quad \text{on } \partial\Omega_{\mathrm{S}} \tag{1.b}$$

where $\vec{E}^{inc}$ and $\vec{E}^s$ are the incident plane wave and scattered field, respectively. Moreover, Ω_{FS} and $\partial\Omega_{\mathrm{S}}$ denote the free-space and the boundary of the scatterer, respectively. It is worthwhile mentioning that (1) is also applicable inside the PML region (Ω_{PML}), except for the fact that the real coordinates are just replaced by their complex counterparts calculated via a special complex coordinate transformation, which is defined in the locally conformal PML method.

In the conventional (or classical) FEM approach employing tetrahedral edge elements, the vector wave equation in (1.a) is not solved directly; instead, it is transformed into its weak variational form using the weighted residual method as follows

$$\int_{\Omega} (\nabla \times \vec{E}^s) \cdot (\nabla \times \vec{W}) d\Omega - k^2 \int_{\Omega} \vec{E}^s \cdot \vec{W} d\Omega = 0 \tag{2}$$

where $\vec{W}$ is a vector weight function. Within each element e, the unknown field is approximated as

$$\vec{E}^{s,e}(\vec{r}) = \sum_{i=1}^{6} \vec{N}_i(\vec{r}) E_i^e \tag{3}$$

where E_i^e is the unknown tangential field along the ith edge, and $\vec{N}_i(\vec{r})$ is the vector shape function for the ith edge. Next, we substitute (3) into (2), and choose the weight functions to be equal to the shape functions (i.e., $\vec{W} = \vec{N}_i(\vec{r})$). After this step, the weak variational form becomes

$$\int_{\Omega^e} \left[\nabla \times \left(\sum_{i=1}^{6} \vec{N}_i(\vec{r}) E_i^e \right) \right] \cdot (\nabla \times \vec{N}_j(\vec{r})) d\Omega - k^2 \int_{\Omega^e} \left(\sum_{i=1}^{6} \vec{N}_i(\vec{r}) E_i^e \right) \cdot \vec{N}_j(\vec{r}) d\Omega = 0 \quad (j = 1, 2, \ldots, 6) \tag{4}$$

Using (4), we construct the 6 × 6 local elemental matrices, which are assembled over all elements to form the global system of equations by using the edge connectivity knowledge of the elements. Specifically, the FEM formulations lead to the following sparse global matrix system

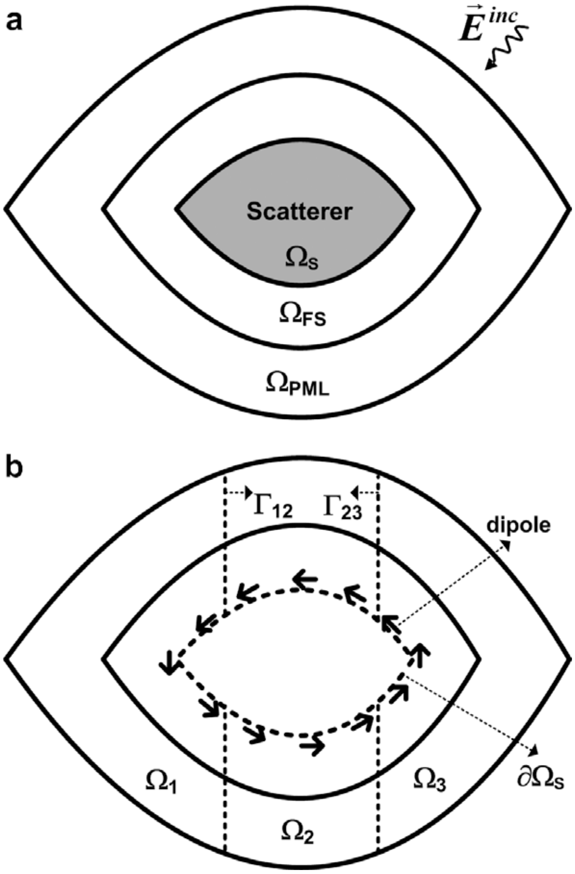

Fig. 1. (a) Original scattering problem; (b) CBFEM-MPI approach.

$$[A][e] = [b] \tag{5}$$

where the elements of the unknown vector $[e]$ are the scalar tangential fields along the edges, $[A]$ is the global matrix and $[b]$ is the known right-hand-side (RHS) vector, which is obtained by the imposing the BCs. The details of the FEM solution of the vector wave equation can be found in [19].

2.1. CBFEM-MPI formulation

The major goal of the CBFEM algorithm is to efficiently solve the same matrix system as that employed in the conventional FEM. Thus, the first step in the CBFEM algorithm is to construct the global matrix system in (5), which corresponds to the original problem at hand. The CBFEM-MPI approach achieves the efficient solution of the matrix system in (5) by decomposing the entire computational domain into a number of *non-overlapping* subdomains, and by employing the CBFs that are *specially* tailored to each subdomain. In this non-iterative and parallelizable technique, the unknown tangential fields are expressed as a series of two types of CBFs, which are weighted with unknown coefficients yet to be determined. Of these CBFs, the first are constructed inside the subdomains, whereas the second are defined on the interfaces. In other words, the unknowns are treated separately on each individual subdomain and interface. Next, the Galerkin method, which employs the CBFs as both basis and testing functions, is realized to transform the global matrix system into a "smaller" matrix, which we call as the reduced-matrix. The most appealing feature of the proposed approach is that the reduced-matrix can still be solved by direct solvers (such as the LU factorization), even if the original problem size is very large. Therefore, in contrast to iterative solvers, multiple right-hand-side vectors (i.e., multiple illuminations in the scattering problem) can be handled efficiently in CBFEM with little additional computational burden. After solving the reduced-matrix for the unknown coefficients, the tangential fields inside the entire computational domain are obtained by substituting the coefficients into the series expressions.

Without loss of generality, we illustrate the CBFEM-MPI technique using the cross-sectional model as shown in Fig. 1(b), which is simply the equivalent of that in Fig. 1(a). We begin by suitably partitioning the original computation domain into a number of subdomains. The subdomains may be created by employing various partitioning schemes, such as by slicing the entire domain along a single direction, or by applying a puzzle-like division. However, the type of the partitioning scheme should be selected carefully for the geometry at hand to minimize the size of the reduced-matrix, because different schemes may generate different number of interface edges, which are directly linked with the size of the reduced-matrix (this will be evident from the discussion in Section 2.1.3). Our next step is to place a finite number (M) of *fictitious dipoles*—or current-elements in general—on the boundary of the scatterer, as illustrated by the black arrows in Fig. 1(b).

The fields that are radiated by these dipoles can be conveniently used as CBFs because they not only form the *natural* basis functions for the field distribution inside the entire computational domain, but they also incorporate the physics of the problem. The theoretical basis of the CBFEM-MPI approach is briefly discussed in Appendix A. It is useful to remark that the concept of fictitious sources has also been used in a number of integral-equation-based numerical techniques for efficient solution of electromagnetic problems. For instance, the Fast Multipole Method expands the Green's function using a multipole expansion, which groups sources that lie close together and treat them as if they are a single source, and accelerates the matrix-vector multiplications needed in the iterative solvers in an efficient manner [20]. Furthermore, in the Discrete Sources Method, an unknown field in a domain under consideration is presented as a finite linear combination of the fields of some fictitious discrete sources placed outside this domain [21].

In the CBFEM-MPI algorithm, the dipoles can easily be chosen to lie along the edges of the usual finite element mesh pertaining to the boundary of the object (see Fig. 2(a)). Specifically, the directions of the dipoles are selected along the unit vectors that denote the directions of the tangential fields along the edges of the elements—shown in Fig. 2(b)—located on the boundary of the scatterer. Thus, it is evident that the task of determining the positions of the dipoles does not require an additional effort, since it is incorporated into the nature of the FEM. Even if the number of dipoles that are chosen along the boundary is large, as is the case of 'large' objects or fine meshes, the number of *effective* dipoles is limited by using a technique, which selects the most contributing dipoles for each point under consideration, as well as by employing the singular value decomposition (SVD) approach with a threshold to reduce the redundancy in the CBFs created by the dipoles (see below).

The CBFEM-MPI algorithm has 3 main steps, and they are described below.

2.1.1. Generation of CBFs along interfaces (Step-1)

We first determine the CBFs (or excitation functions), along each *individual* interface (Γ_ψ), which has *no* common edges with all other interfaces. Clearly, we obtain the CBFs along each 'dual-' (e.g. Γ_ψ where $\psi = \{12,23\}$ in Fig. 1(b)), 'triple-' and 'quadruple-' interfaces where two, three and four subdomains intersect, respectively. It is useful to note that the mesh partitioning algorithm of the CBFEM-MPI has been developed in such a way that at most four subdomains can intersect. In order to find the CBFs, we first compute the fields of the dipoles, which radiate in the *absence* of the scatterer, at the *mid-points of the edges* located on the interfaces. The field created by an arbitrarily oriented dipole inside the free-space, as well as in the PML region, is briefly formulated in Appendix B, for the sake of completeness. While calculating the field at each point on an individual interface, we do *not* consider all the dipoles, but only the *pioneering* dipoles that are located nearest to that interface. More specifically, if the interface under consideration has N_{Γ_ψ} points (i.e., mid-points of the edges), then, for each point, we choose at most N_{Γ_ψ} number of dipoles that are closest to that point. This is because the dipoles that are located at a distance far away from an interface have a negligible effect on that interface, when compared to the effects of the dipoles that are very close to that interface. Another reason is that we employ the SVD approach with a threshold to reduce the redun-

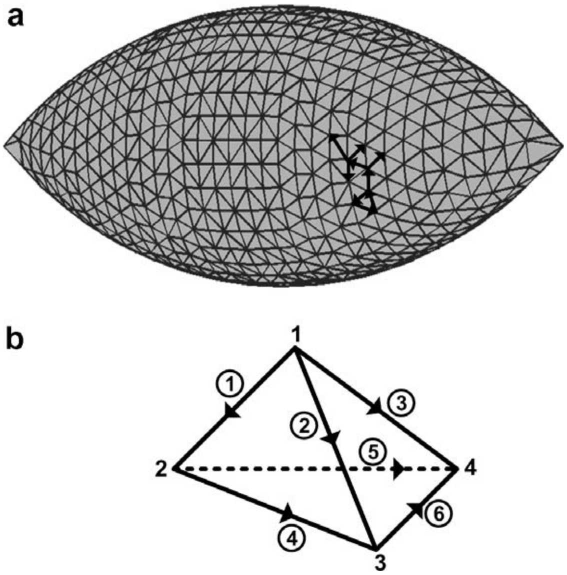

Fig. 2. (a) Illustration of dipole positions on the boundary of object; (b) tetrahedral edge element.

dancy in the basis functions, and the SVD procedure retains at most N_{Γ_ψ} basis functions if the number of dipoles is larger than the number of interface points. This dipole selection scheme helps to decrease the number of dipoles, and thus, the redundancy in the basis functions prior to the application of the SVD procedure. The salutary feature of this scheme becomes more clearly evident if the total number of dipoles is much larger than the number of points on each individual interface (i.e., $M \gg N_{\Gamma_\psi}$), which usually occurs for electrically large objects.

After determining the pioneering dipoles for each interface, we calculate the initial CBFs $[E^{(i)}_{\Gamma_\psi}]$ on each individual interface, where the superscript (i) refers to the ID of the dipole. It is worthwhile to add this remark here that these functions refer to the *scalar* tangential fields along the edges located on the interfaces. Specifically, the vector field along each edge is represented by the multiplication of the scalar function by the unit vector directed along that edge. Then, we apply the SVD procedure to remove the redundancy in the CBFs, by orthogonalizing them. We first let

$$[\Sigma_{\Gamma_\psi}]_{N_{\Gamma_\psi}\times M_\psi} = \left(\left[E^{(1)}_{\Gamma_\psi}\right]\middle|\left[E^{(2)}_{\Gamma_\psi}\right]\middle|\cdots\middle|\left[E^{(M_\psi)}_{\Gamma_\psi}\right]\right)_{N_{\Gamma_\psi}\times M_\psi} \tag{6}$$

where N_{Γ_ψ} is the number of points along each interface Γ_ψ, and M_ψ is the number of pioneering dipoles, which is usually equal to N_{Γ_ψ} as mentioned above. Using the SVD procedure, (6) can be expressed as

$$[\Sigma_{\Gamma_\psi}]_{N_{\Gamma_\psi}\times M_\psi} = [U_{\Gamma_\psi}]_{N_{\Gamma_\psi}\times M_\psi}[\Lambda_{\Gamma_\psi}]_{M_\psi\times M_\psi}[V_{\Gamma_\psi}]^{\mathrm{T}}_{M_\psi\times M_\psi} \tag{7}$$

The ordered singular values of $[\Sigma_{\Gamma_\psi}]_{N_{\Gamma_\psi}\times M_\psi}$ are basically the entries of the diagonal matrix $[\Lambda_{\Gamma_\psi}]_{M_\psi\times M_\psi} = diag(\sigma_1,\sigma_2,\ldots,\sigma_{M_\psi})$. We retain the entries whose singular values are above a threshold. In other words, we retain the first K_{Γ_ψ} ($K_{\Gamma_\psi} < M_\psi$) CBFs such that $\sigma_1,\sigma_2,\ldots,\sigma_{K_{\Gamma_\psi}} < \sigma_{thresh}$. We have found that a choice of the SVD threshold in the range from 1e-4 to 1e-5, yields accurate results. The reduced-matrix starts becoming ill-conditioned if the SVD threshold is decreased much below 1e-6. Finally, we express the post-SVD CBFs associated with each interface as follows

$$[U_{\Gamma_\psi}]_{N_{\Gamma_\psi}\times K_{\Gamma_\psi}} = \left(\left[u^{(1)}_{\Gamma_\psi}\right]\middle|\left[u^{(2)}_{\Gamma_\psi}\right]\middle|\cdots\middle|\left[u^{(K_{\Gamma_\psi})}_{\Gamma_\psi}\right]\right)_{N_{\Gamma_\psi}\times K_{\Gamma_\psi}} \tag{8}$$

This step can be performed in parallel for each individual interface.

2.1.2. Generation of CBFs in subdomains (Step-2)

We construct the CBFs in each subdomain by solving the vector wave equation, with certain excitation functions located on the boundaries of the subdomain, and there are two alternate ways for constructing these functions. One possible approach is to use some combinations of the post-SVD CBFs derived in Step-1. Another approach, which is more efficient than the above, is to determine new excitation functions along the boundaries of each subdomain using a similar procedure given in Step-1. Clearly, we find the points on the boundary of the jth subdomain by concatenating the points on the interfaces where the jth subdomain has been terminated (i.e., $\Gamma_j = \cup_\psi \Gamma_\psi$ where $\Gamma_\psi \subset \Omega_j$). Following the procedure in Step-1, for the jth subdomain, we compute K_{Γ_j} number of post-SVD excitation functions along Γ_j using the pioneering dipoles corresponding to that interface, as follows

$$[U_{\Gamma_j}]_{N_{\Gamma_j}\times K_{\Gamma_j}} = \left(\left[u^{(1)}_{\Gamma_j}\right]\middle|\left[u^{(2)}_{\Gamma_j}\right]\middle|\cdots\middle|\left[u^{(K_{\Gamma_j})}_{\Gamma_j}\right]\right)_{N_{\Gamma_j}\times K_{\Gamma_j}} \tag{9}$$

where N_{Γ_j} is the number of points along Γ_j. Next, we solve the vector wave equation by using the excitation functions in (9) to find K_{Γ_j} number of CBFs that span the jth subdomain. That is, in the jth subdomain, we solve the following sub-problem for each $[u^{(i)}_{\Gamma_j}]$ along the boundary Γ_j ($i = 1,2,\ldots,K_{\Gamma_j}$)

$$\begin{aligned}&\nabla\times\nabla\times\vec{E}^s_j - k^2\vec{E}^s_j = 0 \\ &\text{BCs}: \hat{n}\times\vec{E}^s_j = \left[u^{(i)}_{\Gamma_j}\right]\hat{a}_{\Gamma_j} \quad \text{on } \Gamma_j \\ &(\text{and global BCs in } (1.\text{b}))\end{aligned} \tag{10}$$

where $\hat{a}_{\Gamma_j}$ refers to the unit vector directed along each edge on Γ_j. It is obvious that only the RHS vector corresponding to the new BC need be modified to calculate each new solution. Hence, multiple RHS vectors can be handled efficiently by first utilizing the LU decomposition, and then using only forward and backward substitutions, without using Gaussian elimination each time. Then, the initial CBFs in each subdomain can be expressed as follows

$$[\Sigma_j]_{N_j\times K_{\Gamma_j}} = \left(\left[E^{(1)}_j\right]\middle|\left[E^{(2)}_j\right]\middle|\cdots\middle|\left[E^{(K_{\Gamma_j})}_j\right]\right)_{N_j\times K_{\Gamma_j}} \tag{11}$$

where N_j is the number of points inside the jth subdomain, excluding its boundaries. Next, we resort to the SVD technique once again to make sure that the resulting reduced-matrix is well-conditioned. The SVD approach transforms (11) into the following form

$$[\Sigma_j]_{N_j\times K_{\Gamma_j}} = [U_j]_{N_{\Gamma_j}\times K_{\Gamma_j}}[\Lambda_j]_{K_{\Gamma_j}\times K_{\Gamma_j}}[V_j]^{\mathrm{T}}_{K_{\Gamma_j}\times K_{\Gamma_j}} \tag{12}$$

After retaining the first K_j number of CBFs in a way such that the singular values of (12) are below a threshold value, the final post-SVD CBFs for the jth subdomain become

$$[U_j]_{N_j\times K_j} = \left(\left[u_j^{(1)}\right]|\left[u_j^{(2)}\right]|\ldots|\left[u_j^{(K_j)}\right]\right)_{N_j\times K_j} \tag{13}$$

In common with Step-1, the SVD thresholds in this step can be set to either 1e−4 or 1e−5 to get accurate results. This step can also be realized in parallel for each subdomain.

It is useful to note that the last SVD operation, which is applied to the CBFs inside the subdomains and given in (12), may be eliminated by using an *ad-hoc* approach, outlined below, to reduce the computation time. However, we should emphasize again that this SVD operation guarantees the well-conditioned nature of the reduced-matrix, and thus the accuracy of the results, in all situations. The last SVD procedure can be bypassed by first increasing the threshold value of the SVD operation that is applied to find the excitation functions given in (9), and then choosing the first $K_j < K_{\Gamma_j}$ number of basis functions from the set expressed in (11). The reason for the selection of the first K_j bases is that the basis functions have already been sorted out in (9) with respect to their singular values. In this approach, the SVD threshold that is used in (9) can be increased, for example, to 1e−3, to increase the independency of the basis functions, as well as to decrease their numbers. In addition, K_j can be set to a ratio of K_{Γ_j}, such as 85–95%. Since this approach may yield somewhat less-accurate results—depending on the values of these parameters—a compromise should be made between the computation time and the desired accuracy.

2.1.3. Construction of the reduced-matrix system (Step-3)

Let us now assume that we have three subdomains and two individual interfaces (i.e, $\Gamma_{\psi 1}$ and $\Gamma_{\psi 2}$), for the sake of simplicity. Then, the system of linear equations in (5) can be arranged by treating the entries for each subdomain and interface separately, as follows

$$\begin{bmatrix} [A_{11}] & [0] & [0] & [A_{1\Gamma_{\psi 1}}] & [A_{1\Gamma_{\psi 2}}] \\ [0] & [A_{22}] & [0] & [A_{2\Gamma_{\psi 1}}] & [A_{2\Gamma_{\psi 2}}] \\ [0] & [0] & [A_{33}] & [A_{3\Gamma_{\psi 1}}] & [A_{3\Gamma_{\psi 2}}] \\ [A_{\Gamma_{\psi 1}1}] & [A_{\Gamma_{\psi 1}2}] & [A_{\Gamma_{\psi 1}3}] & [A_{\Gamma_{\psi 1}\Gamma_{\psi 1}}] & [A_{\Gamma_{\psi 1}\Gamma_{\psi 2}}] \\ [A_{\Gamma_{\psi 2}1}] & [A_{\Gamma_{\psi 2}2}] & [A_{\Gamma_{\psi 2}3}] & [A_{\Gamma_{\psi 2}\Gamma_{\psi 1}}] & [A_{\Gamma_{\psi 2}\Gamma_{\psi 2}}] \end{bmatrix} \begin{bmatrix} [e_1] \\ [e_2] \\ [e_3] \\ [e_{\Gamma_{\psi 1}}] \\ [e_{\Gamma_{\psi 2}}] \end{bmatrix} = \begin{bmatrix} [b_1] \\ [b_2] \\ [b_3] \\ [b_{\Gamma_{\psi 1}}] \\ [b_{\Gamma_{\psi 2}}] \end{bmatrix} \tag{14}$$

where each $[A_{\alpha\beta}]$ represents the coupling between the unknowns in the inner part of the αth subdomain or interface, and the unknowns in the inner part of the βth subdomain or interface. In this section, α and β are assumed to be 'dummy' subscripts corresponding to the subdomain and/or interface IDs. We note that the sub-matrices in (14) do not overlap with each other.

The next step is to express the unknowns (i.e., tangential fields) in the each subdomain and on each interface as a weighted sum of CBFs derived in Step-1 and 2, respectively, in terms of a set of coefficients yet to be determined, as follows

$$[e_j]_{N_j\times 1} = \sum_{i=1}^{K_j} c_j^{(i)}\left[u_j^{(i)}\right]_{N_j\times 1} \tag{15}$$

$$[e_{\Gamma_\psi}]_{N_{\Gamma_\psi}\times 1} = \sum_{i=1}^{K_{\Gamma_\psi}} c_{\Gamma_\psi}^{(i)}\left[u_{\Gamma_\psi}^{(i)}\right]_{N_{\Gamma_\psi}\times 1} \tag{16}$$

where $c_j^{(i)}$ and $c_{\Gamma_\psi}^{(i)}$ are the weight coefficients of the CBFs belonging to each subdomain and interface, respectively.

Next, we utilize the Galerkin approach to derive the reduced-matrix. We first substitute (15) and (16) into the matrix system in (14) to find an over-determined system. Then, we left-multiply both sides of this system by $diag([U_1]^{\mathrm{T}}, [U_2]^{\mathrm{T}}, [U_3]^{\mathrm{T}}, [U_{\Gamma_{\psi 1}}]^{\mathrm{T}}, [U_{\Gamma_{\psi 2}}]^{\mathrm{T}})$ to get the reduced-matrix system as follows

$$[S]\begin{bmatrix} [c_1]_{K_1\times 1} \\ [c_2]_{K_2\times 1} \\ [c_3]_{K_3\times 1} \\ [c_{\Gamma_{\psi 1}}]_{K_{\Gamma_{\psi 1}}\times 1} \\ [c_{\Gamma_{\psi 2}}]_{K_{\Gamma_{\psi 2}}\times 1} \end{bmatrix} = \begin{bmatrix} [g_1]_{K_1\times 1} \\ [g_2]_{K_2\times 1} \\ [g_3]_{K_3\times 1} \\ [g_{\Gamma_{\psi 1}}]_{K_{\Gamma_{\psi 1}}\times 1} \\ [g_{\Gamma_{\psi 2}}]_{K_{\Gamma_{\psi 2}}\times 1} \end{bmatrix} \tag{17}$$

where $[S]$ is a $K\times K$ reduced-matrix whose structure is in the same form of $[A]$ given in (14). Here, the matrix size is $K = \left(\sum_\psi K_{\Gamma_\psi} + \sum_{j=1}^{N_d} K_j\right)$, where N_d is the number of subdomains. Each sub-matrix of $[S]$ is computed by

$$[S_{\alpha\beta}]_{K_\alpha\times K_\beta} = [U_\alpha]^{\mathrm{T}}_{K_\alpha\times N_\alpha}[A_{\alpha\beta}]_{N_\alpha\times N_\beta}[U_\beta]_{N_\beta\times K_\beta} \tag{18}$$

Also, each entry of the new RHS vector in (17) is obtained by

$$[g_\alpha]_{K_\alpha\times 1} = [U_\alpha]^{\mathrm{T}}_{K_\alpha\times N_\alpha}[b_\alpha]_{N_\alpha\times 1} \tag{19}$$

At this stage, it is convenient to further reduce the size of the reduced-matrix by utilizing the Schur-complement approach [22], which decouples the unknowns on the interfaces. Therefore, the size of the reduced-matrix using the Schur approach is equal to the total number CBFs along the interfaces. Although the *sparse* reduced-matrix equation in (17) is usually small enough to solve it by using direct solvers, the Schur approach is suggested since it parallelizes the solution of the reduced-matrix, and thus, realizes direct solution techniques in a time-efficient manner, which is obviously useful in handling larger problems. Prior to the application of the Schur-complement approach, the matrix system in (17) can be arranged by concatenating the interface unknowns as shown below

$$\begin{bmatrix} [S_{11}] & [0] & [0] & [S_{1\Gamma}] \\ [0] & [S_{22}] & [0] & [S_{2\Gamma}] \\ [0] & [0] & [S_{33}] & [S_{3\Gamma}] \\ [S_{\Gamma 1}] & [S_{\Gamma 2}] & [S_{\Gamma 3}] & [S_{\Gamma\Gamma}] \end{bmatrix} \begin{bmatrix} [c_1]_{K_1\times 1} \\ [c_2]_{K_2\times 1} \\ [c_3]_{K_3\times 1} \\ [c_\Gamma]_{K_\Gamma\times 1} \end{bmatrix} = \begin{bmatrix} [g_1]_{K_1\times 1} \\ [g_2]_{K_2\times 1} \\ [g_3]_{K_3\times 1} \\ [g_\Gamma]_{K_\Gamma\times 1} \end{bmatrix} \tag{20}$$

where $\Gamma = \cup_\psi \Gamma_\psi$. The Schur-complement system for (20) is given by

$$[P][c_\Gamma] = [y] \tag{21}$$

where

$$[P] = [S_{\Gamma\Gamma}] - \sum_{i=1}^{N_d} [S_{\Gamma i}][S_{ii}]^{-1}[S_{i\Gamma}] \tag{22}$$

$$[y] = [g_\Gamma] - \sum_{i=1}^{N_d} [S_{\Gamma i}][S_{ii}]^{-1}[g_i] \tag{23}$$

After solving (21) for the unknown coefficients corresponding to the interfaces, the unknown coefficients for each subdomain can be calculated by solving the following matrix system

$$[S_{ii}][c_i] = [h_i] \tag{24}$$

where

$$[h_i] = [g_i] - [S_{i\Gamma}][c_\Gamma] \tag{25}$$

The system of equations in (24) can be solved in a parallel manner. We should add a final remark here that although the matrices in (21) and (24) are denser than the reduced-matrix in (17), they are smaller and better-conditioned, thus, can be conveniently handled by performing full-matrix direct solvers. Final step is to substitute the computed coefficients into (15) and (16), and to obtain the field distribution inside the entire domain.

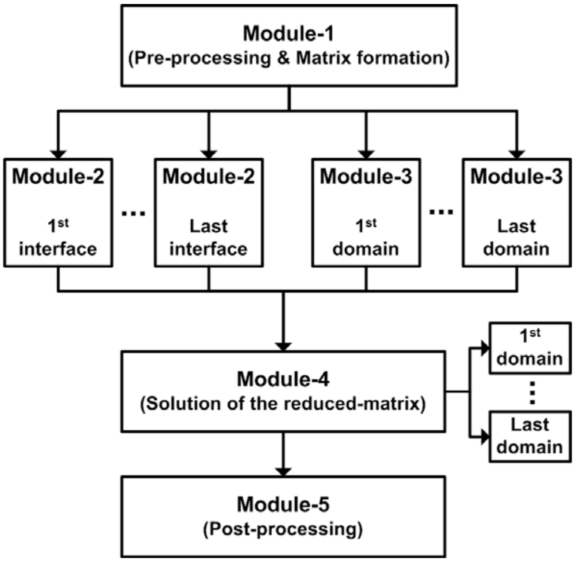

Fig. 3. Parallel architecture of CBFEM-MPI.

2.2. Parallel architecture of the CBFEM-MPI

The CBFEM-MPI algorithm has been parallelized in the C language using the Message Passing Interface (MPI) library [11], which is a library standard to perform parallel processing techniques using a distributed-memory model. In the CBFEM-MPI code, the *master* process is responsible for distributing the parallel jobs to the available processors (*slaves*), and for the task-timing in the code sequence. Multiple slave processes communicate with the master process through the MPI routines (such as MPI_Recv, MPI_Send, etc.) and certain data files. The CBFEM-MPI algorithm can be divided into five main phases, called *modules*, as illustrated in Fig. 3. Initially, Module-1 performs the mesh generation and partitioning algorithms using tetrahedral edge elements, and constructs the global and sub-matrices, which are given in (14), in compressed sparse row (CSR) format. Then, the Modules 2 and 3 realize the Steps 1 and 2 in parallel for each interface and subdomain, respectively, and can be initiated concurrently. The Module-4, corresponding to Step-3, can also be parallelized, for each subdomain, in the solution of sub-matrices given in (24). Finally, in Module-5, the radar cross-section (RCS) is calculated using the field distribution inside the entire computational domain.

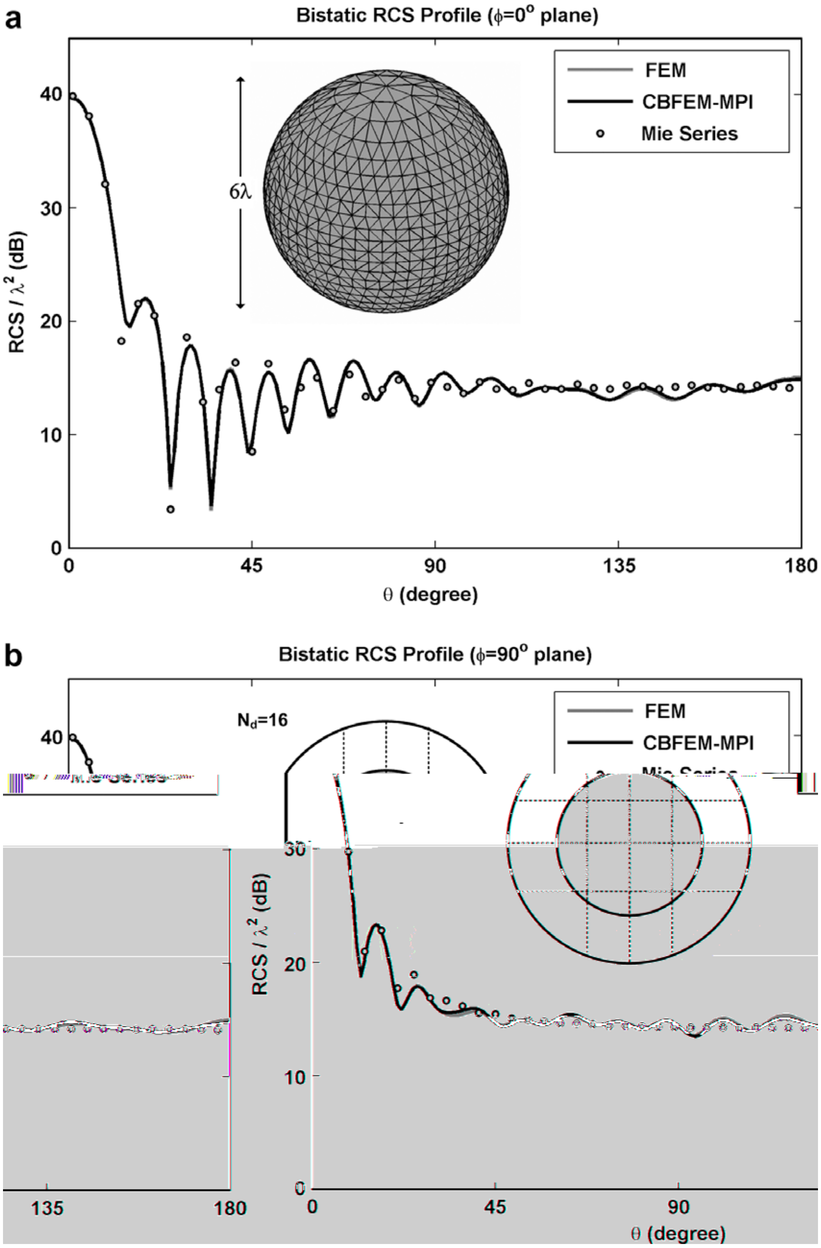

Fig. 4. Bistatic RCS profile of sphere: (a) $\phi = 0°$ plane and (b) $\phi = 90°$ plane.

Table 1
Number of CBFs in each subdomain for sphere.

	Ω_1	Ω_2	Ω_3	Ω_4	Ω_5	Ω_6	Ω_7	Ω_8
Pre-SVD	1858	2094	2093	1861	2348	1784	1790	2367
Post-SVD	1355	1724	1714	1361	1573	1325	1324	1603
	Ω_9	Ω_{10}	Ω_{11}	Ω_{12}	Ω_{13}	Ω_{14}	Ω_{15}	Ω_{16}
Pre-SVD	2345	1766	1778	2363	1858	2088	2090	1855
Post-SVD	1527	1307	1311	1581	1354	1722	1717	1361

3. Numerical examples

In this section, we present the results of some numerical experiments to test the performance of the CBFEM-MPI technique in 3D scattering problems. In these examples, we employ an FEM mesh generated by using tetrahedral edge elements whose edge size is approximately set to $\lambda/10$, assuming that the wavelength λ is 1 m. In the CBFEM-MPI code, we have utilized the LAPACK[2] and SuperLU[3] packages to realize full and sparse matrix operations, respectively.

The first example is a benchmark scattering problem where a plane wave, $\vec{E}^{inc} = \hat{a}_x \exp(-jkz)$, is incident to a sphere whose diameter is 6λ. The original domain is partitioned into 16 subdomains, as shown in the figure that is the inset of Fig. 4. This partitioning scheme creates 16,064 edges pertaining to the interfaces. For the original problem, the number of unknowns (edges or matrix size) is 313,958. Total number of dipoles chosen along the boundary of the sphere is 13,828. The CBFEM-MPI code yields a reduced-matrix whose size is 16,016, which is considerably less than the original matrix size, when the Schur-complement approach is implemented. The size of the reduced-matrix also represents the total number of CBFs along the interfaces. The number of CBFs used in the subdomains is tabulated in Table 1 to better grasp how small the matrices given in (22) and (24) are, so that they can conveniently be handled while performing the direct solution and inverse operations. Finally, the bistatic RCS profile of the sphere is plotted in Fig. 4, which also compares it with both the conventional FEM and the Mie series results [23]. The profiles of the CBFEM-MPI are very close to those of the conventional FEM. Also, we point out that although there are small discrepancies between the profiles of the CBFEM-MPI and the Mie series, they can be improved by refining the mesh. It is worthwhile to note that it is more realistic to compare the CBFEM-MPI results with those computed by the conventional FEM to measure the performance of the proposed algorithm, because the main concern of the present method is to efficiently solve the same matrix system as that employed in the conventional FEM. For this purpose, we can also compute the mean-square percentage difference (i.e., $\mathrm{Err} = \sum_{\Omega}|E^{\mathrm{CBFEM}} - E^{\mathrm{FEM}}|^2/\sum_{\Omega}|E^{\mathrm{FEM}}|^2$) between the field distributions (i.e., tangential fields along the edges) of the conventional FEM and the CBFEM-MPI inside the "entire" computational domain to show that CBFEM-MPI fully recovers the original solution (namely, the solution of the conventional FEM) in both near- and far-field. In this example, we find that the percentage difference is on the order of 0.4876%.

The second example considers the problem of scattering from a cube whose edge length is 5λ, assuming that the incident plane wave is $\vec{E}^{inc} = \hat{a}_y \exp(-jkz)$. The entire domain is partitioned into 24 subdomains (see the inset of Fig. 5), yielding 19,405 interface edges. The original matrix size is 624,462. The CBFEM-MPI code employs 23,600 dipoles located along the boundary of the cube. The size of the reduced-matrix constructed via the Schur approach is only 19,006. The bistatic RCS profile is plotted in Fig. 5, together with the measured results given in [24].

The third example deals with a missile whose radome diameter is 2λ and length is 21λ, with an axial (nose-on) plane wave incidence ($\vec{E}^{inc} = \hat{a}_y \exp(jkz)$). The computational domain is decomposed into 25 subdomains, as shown in Fig. 6, generating 23,003 interface edges. The number of unknowns in this problem is 563,147, and the number of dipoles is 39,582. The size of the reduced-matrix is obtained as 22,706. We plot the bistatic RCS profile in Fig. 6, and compare the results with those calculated by the forward–backward domain decomposition method proposed in [9].

The fourth example involves the problem of scattering from a square plate whose edge length is 10λ, with a normal plane wave incidence ($\vec{E}^{inc} = \hat{a}_y \exp(jkz)$). The original problem, which has 845,643 unknowns, is divided into 32 subdomains, as shown in Fig. 7. The number of dipoles on the boundary of the plate is 19,041. The CBFEM-MPI algorithm reduces the matrix size into 24,225. The bistatic RCS profile is plotted in Fig. 7, which is compared with the Physical Optics (PO) method, as well as the forward–backward domain decomposition method given in [9]. It is well-known that the PO method is only reliable for aspect angles in the range $\theta \leqslant 20^\circ$.

Finally, we present the results of the scattering problem involving two spheres, which are oriented as in Fig. 8, to illustrate that the CBFEM-MPI method can also be applied for multiple-scatterers in a straightforward manner. The diameter of each sphere is 1λ, and the separation between the spheres is 0.5λ. The original problem is partitioned into 4 subdomains. The number of dipoles on the boundaries of the spheres is 5232. The original matrix size is 108,057, whereas the size of the reduced-matrix is 2903. We plot the bistatic RCS profile in Fig. 8, which also compares it with the conventional FEM result. In

[2] http://www.netlib.org/clapack/.

[3] http://crd.lbl.gov/~xiaoye/SuperLU/.

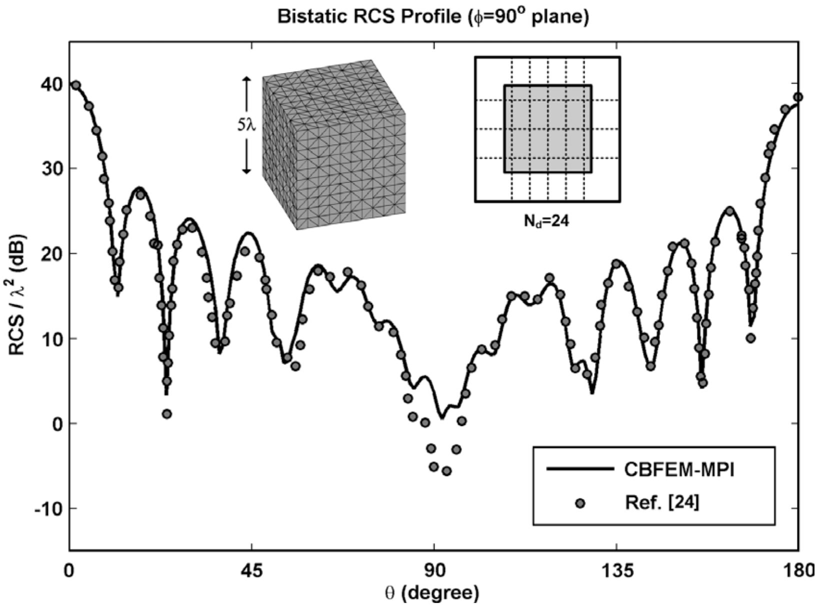

Fig. 5. Bistatic RCS profile of cube at $\phi = 90^\circ$ plane.

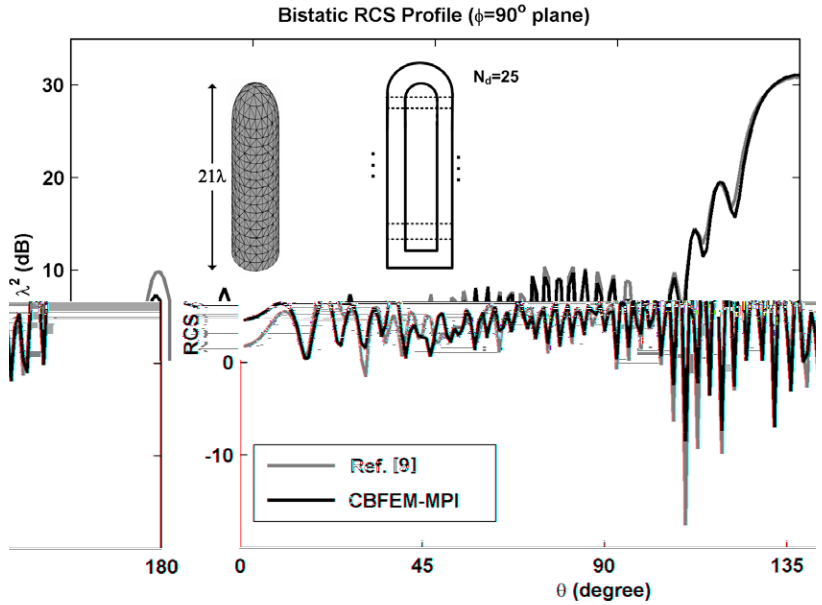

Fig. 6. Bistatic RCS profile of missile at $\phi = 90^\circ$ plane.

this example, we have again computed the percentage difference between the field distributions of the CBFEM-MPI and the conventional FEM, and have found it to be only 0.4596%.

The numerical results in this section demonstrate that the CBFEM-MPI has the ability to reduce the matrix size substantially. We observe that its results are close to the reference results, and this leads us to conclude that the accuracy of the algorithm is validated. Finally, in order to give an idea about the time-efficiency of the algorithm, the CPU time for the last example, which is indeed the smallest example in this section, is 13 min on a LINUX 2.4 GHz cluster with 4 processors. However, it is approximately 5 h for the conventional FEM employing a standard iterative solver (such as biconjugate gradient method). The discrepancy between the relative efficiencies of the two approaches is expected to increase as we increase the number of unknowns, especially when the convergence of the iterative solver is slow, owing to the increase in the condition number of the original matrix. We estimate that the solution of the largest problem (i.e., fourth example), which takes approximately 8.5 h using the CBFEM-MPI code when 32 processors are used, might require several days if we would use

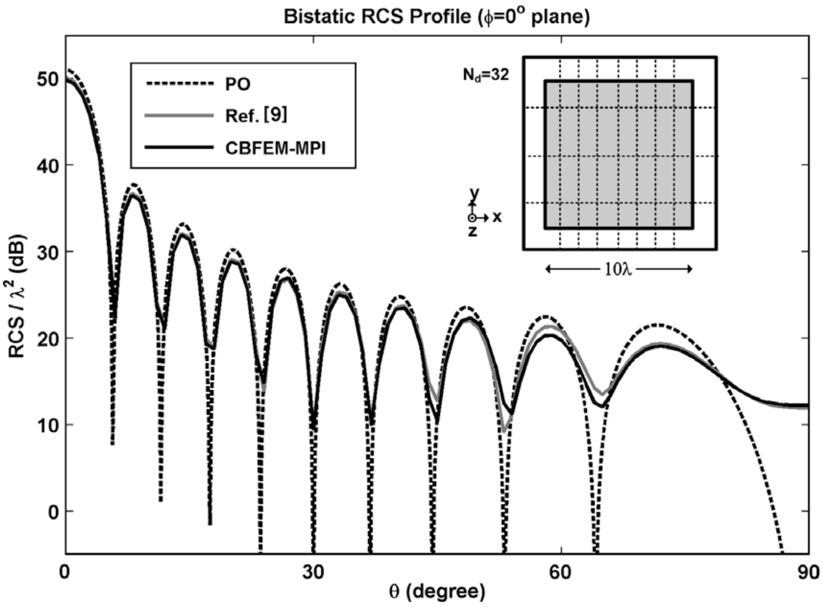

Fig. 7. Bistatic RCS profile of plate at $\phi = 0°$ plane.

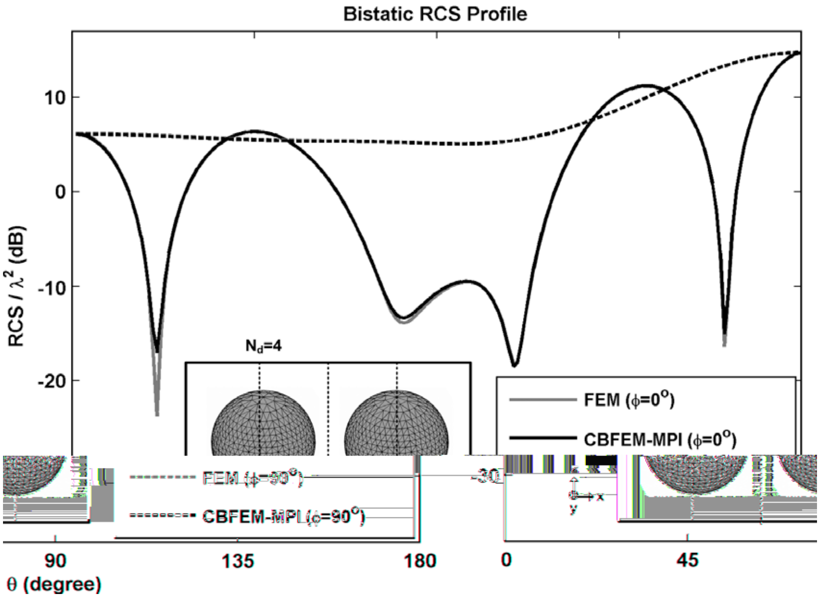

Fig. 8. Bistatic RCS profile of two-spheres.

standard solvers. It is obvious that "small" matrices can be handled by using direct solvers in the conventional FEM. However, for large matrices, it is no longer possible to employ these solvers, and we must resort to iterative solvers instead. Thus, the time comparison, given above, is intended to provide a rough estimate of the relative computational efficiencies of the proposed technique when compared with the conventional FEM employing iterative solvers.

4. Conclusions

We have introduced a novel finite element algorithm for efficient solution of electromagnetic scattering problems, which utilizes the concepts of domain decomposition and characteristic basis functions. We have proposed a new procedure for systematic calculation of the characteristic basis functions using current-elements located on the boundary of the object. We have presented the parallelized structure of the algorithm via the MPI library, and have shown that the algorithm can be successfully implemented on multiple processors in a time-efficient manner. We have also demonstrated that the most distinctive feature of the proposed algorithm is its capability to achieve a considerable reduction in the matrix size, which, in turn, allows us to make use of the direct rather than iterative solvers that are currently in use. We have presented the results for scattering problems involving a number of relatively large and arbitrarily shaped objects. Finally, we remark that the approach presented in this paper is quite general, and can also applied to problems involving both pure dielectric as well as dielectric-coated PEC objects. The results obtained to-date are quite encouraging and will be published in the near future.

Acknowledgment

This work was supported in part by a grant from The Scientific and Technological Research Council of Turkey (TUBITAK).

Appendix A. This section aims to establish a theoretical basis for the CBFEM-MPI approach. Specifically, it tries to answer why the fields, which are created by the current-elements (i.e., dipoles in 3D and line-sources in 2D) on the scatterer boundary, can be used as the CBFs along the interfaces. The formulations are presented in 2D for the sake of simplicity, and can also be generalized to the 3D case.

By analogy to the 3D scattering problem, the 2D scattering problem can be solved by placing a finite number of line-sources on the surface that originally has been the boundary of the conducting object. Assuming the TM$_z$ mode where only the z-component of the electric field exists, the field values that are created by the line-sources at points along the interfaces are calculated using the following expression [23]

$$E_z(\vec{r}) = -\frac{k\eta}{4} I H_0^{(2)}(k|\vec{r}-\vec{r}'|) \tag{A.1}$$

where $H_0^{(2)}$ is the Hankel function of the second kind of zeroth order (viz., Green's function), η is the intrinsic impedance of the medium, $\vec{r}'$ and $\vec{r}$ are the position vectors of the line-source and interface point, respectively, and I is the current on the line-source.

In order to explain why the fields of the line-sources can be chosen as the basis functions in the CBFEM-MPI approach, it is necessary to express the scattered field outside a conducting object in terms of an integral expression. Let us assume that we have an infinitely long, along z-direction, conducting cylinder of arbitrary cross-section (refer to Fig. 1). The scattered field is denoted by E_z^s, and satisfies the scalar homogeneous Helmholtz equation in the region outside the cylinder

$$\nabla^2 E_z^s + k^2 E_z^s = 0 \tag{A.2}$$

subject to the boundary condition $E_z^s = -E_z^{inc}$ on the boundary of the object ($\partial\Omega_s$), where E_z^{inc} is the incident plane wave.

An alternative formulation can be obtained by using the fact that the incident wave induces currents on the boundary of the cylinder. This current, which can be expressed as $\vec{J} = \hat{a}_z J_z(x,y)$, behaves as the source creating the scattered field. Here, the current density J_z can be expressed as a linear combination of the current-elements ($J_z dl$) on $\partial\Omega_s$. Each current-element creates the following field

$$J_z dl \rightarrow -\frac{k\eta}{4} J_z dl H_0^{(2)}(k|\vec{r}-\vec{r}'|) \tag{A.3}$$

Therefore, using the superposition principle, which is the linear relationship between the scattered field and the current density function, the scattered field is expressed as follows

$$E_z^s = -\frac{k\eta}{4} \oint_{\Omega_s} J_z H_0^{(2)}(k|\vec{r}-\vec{r}'|)dl \tag{A.4}$$

The integral expression in (A.4) can be simplified by approximating the contour $\partial\Omega_s$ in terms of line segments Δl_i, and using finite-width current-elements $J_z^i \Delta l_i$, where J_z^i denotes the value of J_z at the 'center' of the line segment Δl_i, as follows

$$E_z^s \approx -\frac{k\eta}{4} \sum_i J_z^i \Delta l_i H_0^{(2)}(k|\vec{r}-\vec{r}_i'|) \tag{A.5}$$

Thus, the scattered field can be interpreted as a weighted sum of basis functions (i.e., $H_0^{(2)}(k|\vec{r}-\vec{r}_i'|)$) with some coefficients (i.e., $J_z^i \Delta l_i$). In other words, the fields radiated by the current-elements form the *natural* basis functions of the scattered field. Hence, we conclude that the CBFs that are employed in the CBFEM-MPI approach are well-suited to the physics of the problem.

Appendix B. In this section, we present a general formulation regarding the field of an arbitrarily oriented infinitesimal dipole at a point in free-space, as well as inside the PML region. First, we assume that the medium is free-space. The electric field of an infinitesimal dipole that is oriented along z-direction and is of moment Il, where I is the constant current along the dipole and l is the length, is expressed in spherical coordinates as follows [23]

$$E_r = \frac{\eta Il}{2\pi r^2}\left(1+\frac{1}{jkr}\right)\cos\theta\exp(-jkr) \tag{B.1a}$$

$$E_\theta = \frac{jk\eta Il}{4\pi r}\left(1+\frac{1}{jkr}-\frac{1}{(kr)^2}\right)\sin\theta\exp(-jkr) \tag{B.1b}$$

$$E_\phi = 0 \tag{B.1c}$$

These equations can be generalized for a dipole oriented along in an arbitrary direction. We first rotate the dipole by an arbitrary angle α, and express the fields as rotated versions of the original fields in (B.1). In the rotated coordinate system, the new angles (α, β) correspond to the angles (θ, ϕ) in the original spherical coordinate system, where β is referenced to the x-axis. The value of r, which represents the distance between the origin and the point at which the field is to be calculated, is identical in both original and rotated coordinate systems. The transformations of the fields in (B.1) to those in the rotated coordinate system can be simply written as

$$E_r = \frac{\eta Il}{2\pi r^2}\left(1+\frac{1}{jkr}\right)\cos\alpha\exp(-jkr) \tag{B.2a}$$

$$E_\alpha = \frac{jk\eta Il}{4\pi r}\left(1+\frac{1}{jkr}-\frac{1}{(kr)^2}\right)\sin\alpha\exp(-jkr) \tag{B.2b}$$

In order to find the definitions of the terms (cosα,sin α), we use the definition of the dot product

$$\cos\alpha = \hat{a}_r \cdot \hat{a}_d \tag{B.3}$$

where $\hat{a}_r$ and $\hat{a}_d$ are the unit vectors directed along r and the dipole orientation, respectively. Next, we use the following trigonometric identity

$$\sin\alpha = \sqrt{1-\cos^2\alpha} = \sqrt{1-(\hat{a}_r\cdot\hat{a}_d)^2} \tag{B.4}$$

Finally, we substitute (B.3) and (B.4) into (B.2) to calculate the field of the dipole.

Inside the PML region, the above-mentioned approach is followed in the same way to compute the field of the dipole, but except that the field is forced to decay to mimic the wave behavior inside the PML region. This decaying behavior is easily satisfied by using the locally conformal PML method. If the point is inside the PML region, the field in (B.2) is multiplied by a monotonically decreasing exponential function $\exp[-f(\xi)]$, which is equivalent to the true PML action providing an 'artificial decay' inside the PML region. Here, $f(\xi)$ is the same function that is defined in the complex coordinate variations of the locally conformal PML method, and is expressed as

$$f(\xi) = \frac{\alpha\xi^m}{m\|\vec{r}_{\text{out}}-\vec{r}_{\text{in}}\|^{m-1}} \tag{B.5}$$

where ξ is the parameter defined by $\xi = \|\vec{r}-\vec{r}_{\text{in}}\|$, α is a positive parameter and m is a positive integer. Moreover, $\vec{r}_{\text{in}}$ and $\vec{r}_{\text{out}}$ are the position vectors of the points located on the inner $(\partial\Omega_{\text{in}})$ and the outer boundaries of the PML, respectively, where the former is the solution of the minimization problem: $\min_{\vec{r}_{\text{in}}\in\partial\Omega_{\text{in}}}\|\vec{r}-\vec{r}_{\text{in}}\|$. The details of the locally conformal PML technique can be found in [17,18]. It is worthwhile to mention that these computations, which determine the CBFs inside the PML region, do not create any burden in the CBFEM-MPI algorithm, because the above-mentioned parameters are already calculated for each PML point in the matrix construction phase of the algorithm.

References

[1] H. Schwarz, Gesammelte Mathematische Abhandlungen, vol. 2, Springer, Berlin, Germany, 1890. pp. 133–143.

[2] B. Despres, P. Joly, J.E. Roberts, A Domain Decomposition Method for the Harmonic Maxwell Equations, Iterative Methods in Linear Algebra, North-Holland Publishing Co, Amsterdam, 1992, pp. 245–252.

[3] C. Farhat, F.-X. Raux, A method of finite element tearing and interconnecting and its parallel solution algorithms, Int. J. Numer. Methods Eng. 32 (1991) 1205–1227.

[4] B. Stupfel, A hybrid finite element and integral equation domain decomposition method for the solution of 3-D scattering problem, J. Comput. Phys. 172 (2001) 451–471.

[5] C.T. Wolfe, U. Navsariwala, S.D. Gedney, A parallel finite-element tearing and interconnecting algorithm for solution of the vector wave equation with PML absorbing medium, IEEE Trans. Antennas Propag. 48 (2000) 278–284.

[6] V.V. Veremey, R. Mittra, Efficient computation of interconnect capacitances using the domain decomposition approach, IEEE Trans. Adv. Pack. 22 (1999) 348–355.

[7] A. Schadle, L. Zschiedrich, S. Burger, R. Klose, F. Schmidt, Domain decomposition method for Maxwell's equations: scattering off periodic structures, J. Comput. Phys. 226 (2007) 477–493.

[8] X. An, Z.-Q. Lu, A fast algorithm based on partial basic solution vectors domain decomposition method for scattering analysis of electrically large cylinders, J. Comput. Phys. 219 (2006) 930–942.

[9] O. Ozgun, M. Kuzuoglu, Forward–backward domain decomposition method for finite element solution of boundary value problems, Microwave Opt. Technol. Lett. 49 (2007) 2582–2590.

[10] O. Ozgun, M. Kuzuoglu, Finite element analysis of electromagnetic wave problems via iterative leap-field domain decomposition method, J. Electromagn. Waves Appl. 22 (2008) 251–266.

[11] W. Gropp, E. Lusk, A. Skjellum, Using MPI: Portable Parallel Programming with the Message-Passing Interface, MIT Press, Cambridge, 1994.

[12] V.V.S. Prakash, R. Mittra, Characteristic basis function method: a new technique for efficient solution of method of moments matrix equations, Microwave Opt. Technol. Lett. 36 (2003) 95–100.

[13] J. Yeo, V.V.S. Prakash, R. Mittra, Efficient analysis of a class of microstrip antennas using the characteristic basis function method (CBFM), Microwave Opt. Technol. Lett. 39 (2003) 456–464.

[14] G. Tiberi, A. Monorchio, G. Manara, R. Mittra, A spectral domain integral equation method utilizing analytically derived characteristic basis functions for the scattering from large faceted objects, IEEE Trans. Antennas Propag. 54 (2006) 2508–2514.

[15] M. Kuzuoglu, Fast solution of electromagnetic boundary value problems by the characteristic basis functions/FEM approach, in: IEEE Anten. Prop. Soc. Int. Symp., Columbus, OH, vol. 2, June 22–27, 2003, pp. 1072–1075.

[16] H. Abd-El-Raouf, R. Mittra, J.-F. Ma, Solving very large EM problems (10^9 DoFs or greater) using the MPI-CBFDTD method, in: IEEE Anten. Prop. Soc. Int. Symp., Washington DC, vol. 2B, July 3–8, 2005, pp. 2–5.

[17] O. Ozgun, M. Kuzuoglu, Near-field performance analysis of locally-conformal perfectly matched absorbers via Monte Carlo simulations, J. Comput. Phys. 227 (2007) 1225–1245.

[18] O. Ozgun, M. Kuzuoglu, Non-Maxwellian locally-conformal PML absorbers for finite element mesh truncation, IEEE Trans. Antennas Propag. 55 (2007) 931–937.

[19] J. Jin, The Finite Element Method in Electromagnetics, John Wiley & Sons, 2002.

[20] V. Rokhlin, Rapid solution of integral equations of classical potential theory, J. Comput. Phys. 60 (1985) 187–207.

[21] Y. Eremin, N.V. Orlov, A.G. Sveshnikov, Electromagnetic scattering analysis based on discrete sources method, J. Appl. Comput. Electromagn. Soc. 9 (3) (1994) 46–56.

[22] T.N. Philips, Preconditioned iterative methods for elliptic problems on decomposed domains, Int. J. Comput. Math. 44 (1992) 5–18.

[23] C.A. Balanis, Advanced Engineering Electromagnetics, John Wiley & Sons, 1989.

[24] M.G. Cote, M.B. Woodworth, A.D. Yaghijan, Scattering from the perfectly conducting cube, IEEE Trans. Antennas Propag. 36 (1988) 1321–1329.